Supplemental Information

Table S1. CryoEM and model parameters

Data Collection	*GLP-1-GLP-1R-Gs*	*PF-06882961-GLP-1R-Gs*	*OWL833-GLP-1R-Gs*
Magnification	105,000	105,000	105,000
Voltage (kV)	300	300	300
Spot size	4	4	5
Electron exposure (e-/Å^2)	65.4	60.1	54.6
Exposure time (s)	3	3	5
Movie frames	75	75	71
K3 CDS mode	No	No	Yes
Defocus range (μm)	0.6-1.4	0.5-1.3	0.7-1.5
Pixel size (Å)	0.826	0.826	0.826
Symmetry imposed	C1	C1	C1
Final particle imaged (no.)	635,785	683,444	934,493
Resolution (Å)	2.1 (2.2[a], 2.4[b], 2.4[c])	2.5 (2.5[a], 2.8[b], 2.2[c])	2.1 (2.2[a], 2.3[b], 2.8[c])
FSC threshold	0.143	0.143	0.143
Refinement			
Initial model used (PDB code)	6B3J	6X18	6X1A
Map sharpening B factor (Å^2)	-44	-59	-25
Model composition			
Non-hydrogen atoms	10371	10140	10277
Protein residues	1289	1262	1258
ligand	0	1	1
RMSDs			

Bond length (Å)	0.007	0.006	0.007
Bond angles (°)	1.106	0.888	1.032
Validation			
MolProbity score	1.74	2.35	1.75
Clashscore	10.83	13.98	12.45
Rotamer outliers (%)	1.45	3.79	1.01
Ramachandran plot			
Favoured (%)	97.71	96.15	97.26
Allowed (%)	2.21	3.85	2.66
Disallowed (%)	0.08	0	0.08

[a]Resolution (Å) of receptor-focused cryo-EM map

[b]Resolution (Å) of ECD-focused cryo-EM map

[c]Resolution (Å) of complex including the "down" conformation of the $G\alpha_s$ AHD

Table S2: Interactions between the GLP-1R and GLP-1, PF-06882961 or OWL833

GLP-1R Receptor residues		GLP-1	PF-06882961	OWL833
ECD	V30^{ECD}	E21		
	S31^{ECD}	E21	Pyridine	Methyl pyrazolopiperidine
	L32^{ECD}	E21 (H bond) A24 F28	Fluorobenzyl group Ethoxy linker	
	W33^{ECD}		4-cyano-2-fluorobenzyl group (π-π interaction) Pyridine (π-π interaction)	Indole (π-π interaction) Dimethylmorpholine
	E34^{ECD}			Methyl pyrazolopiperidine
	T35^{ECD}	F28 I29		
	V36^{ECD}		4-cyano-2-fluorobenzyl group	
	Q37^{ECD}		4-cyano group	
	W39^{ECD}	F28 (π-π interaction) L32 R36 (π-π interaction)		
	E68^{ECD}	L32 R36		
	Y69^{ECD}	I29 L32 V33		
	P90^{ECD}	I29		
	W91^{ECD}	I29		
	R121^{ECD}	V33 (H bond)		
	E128^{ECD}	K26		
TM1	P137$^{1.32}$	Y19		Methyl pyrazolopiperidine Dimethyl fluorophenyl group Imidazolone

	E138$^{1.33}$	Y19		Dimethyl fluorophenyl group Methyl fluoroindazole
	L141$^{1.36}$	F12	Pyridine	Dimethyl fluorophenyl group
	L144$^{1.39}$	F12		Dimethyl fluorophenyl group
	Y145$^{1.40}$			Dimethyl fluorophenyl group Methyl fluoroindazole (π-π interaction)
	Y148$^{1.43}$	F12 (π-π interaction)	*GLP-1R F385$^{7.40}$ (π-π interaction)*	Dimethyl fluorophenyl group (π-π interaction)
	Y152$^{1.47}$	E9 (H bond)	Carboxylic acid (water mediated)	
TM2	R190$^{2.60}$	E9 (H bond)	Carboxylic acid (water mediated)	
	K197$^{2.67}$	T13 (H bond)	Benzimidazole (H bond)	Imidazolone Indole
	D198$^{2.68}$			Methyl fluoroindazole Imidazolone
	L201$^{2.71}$	V16	Piperidine	Dimethylmorpholine
	K202$^{2.72}$			Methyl fluoroindazole
	W203$^{2.73}$		Piperidine	
	Y205$^{2.75}$	S17 (H bond) L20 E21 (H bond)		Methyl fluoroindazole (π-π interaction)
ECL1	S206^{ECL1}		Fluorobenzyl-oxy group	
	T207^{ECL1}		Fluorobenzyl-oxy group	
	Q210^{ECL1}	A24 E27		

	W214$^{E}_{CL1}$	F28 (π-π interaction) W31 (π-π interaction)		
	L217$^{EC}_{L1}$		4-cyano-2-fluorobenzyl group	
	Y220$^{EC}_{L1}$			Dimethylmorpholine (H bond)
	Q221$^{EC}_{L1}$	E21	4-cyano group Oxetane group	
TM3	C226$^{3.29}$			Dimethylmorpholine
	V229$^{3.32}$			Dimethylmorpholine
	F230$^{3.33}$	T13	Oxetane group Benzimidazole-6-carboxylic acid (π-π interaction)	Dimethylmorpholine Indole (π-π interaction)
	M233$^{3.36}$	T13	Benzimidazole	Dimethylmorpholine
	Q234$^{3.37}$	H7 (H bond)	Carboxylic acid (water mediated)	
	V237$^{3.40}$	H7		
	Y241$^{3.44}$	A8 (water mediated) E9 (water mediated)		
ECL2	C296$^{EC}_{L2}$		Oxetane group	
	T298$^{EC}_{L2}$	G10 (water mediated) T13 S14 S17 (H bond)	4-cyano group	Indole Methylcyclopropyl group Carbonyl group (water mediated)
	R299$^{EC}_{L2}$	S14 S17 (H bond) S18 E21 (H bond)	Carboxylic acid (water mediated)	
	N300$^{EC}_{L2}$	G10 S14 (H bond)		Methylcyclopropyl group
TM5	W306$^{5.36}$	H7 (π-π interaction), G10, T11		
	I309$^{5.39}$	H7		

	R310$^{5.40}$	H7 (water mediated)		
	I313$^{5.43}$	H7		
ECL3	D372^{ECL3}	T11		
TM7	R380$^{7.35}$	T11 D15 (ionic interaction)	Carboxylic acid (ionic interaction)	
	F381$^{7.36}$		Piperidine Benzimidazole (π-π interaction)	
	L384$^{7.39}$	A8 T11 D15	Benzimidazole	
	F385$^{7.40}$		Piperidine	
	E387$^{7.42}$	A8		
	L388$^{7.43}$	A8 E9 (water mediated), F12		Dimethyl fluorophenyl group

Receptor residues within 4 Å of the bound ligand (GLP-1, PF-06882961 or OWL833) are listed. Hydrogen (H) bonds were determined using Ligplot+. Residues in blue are interactions not shown in Ligplot+.

Figure S1. Kinetic profiles of binding, transducer coupling and signalling mediated by GLP-1 and non-peptidic agonists. *Related to Figure 1.* **A,** Agonist-induced changes in trimeric G_s protein conformation measured as a ligand-induced change in BRET between Nluc-$G\alpha_s$ and Venus-$G\gamma$ in membranes prepared from HEK293 cells expressing the GLP-1R. Rates were calculated using a one phase association model; the rate reported was from an approx. EC_{90} concentration of each agonist. **B,** Kinetics of calcium signalling in live HEK293 cells expressing the GLP-1R. **C,** A time-course for pERK1/2 was performed at a single ligand concentration to determine the peak response. This revealed similar profiles of pERK1/2 kinetics, albeit with different maximal signals. **D-E**, Kinetics of β-arrestin-1 (D) and β-arrestin-2 recruitment (E). **F,** Kinetics for ligand-induced BRET between GLP-1R-Rluc8 and the early endosomal marker FYVE-Venus**.** Rates were determined using a one phase association model; the rate reported was from an approx. EC_{90} concentration of each agonist. **G,** Kinetic ligand binding assay in membranes measuring nBRET between Nluc-GLP-1R and the fluorescent probe AF568-GLP-1 in the presence and absence of increasing concentrations of unlabelled agonists. The colour key at the bottom provides information regarding the ligand concentrations used for each ligand in each assay. All experiments were performed in GLP-1R HEK293 cells and with the exception of panel G (n=3), all panels show the mean + S.E.M of 5 independent experiments performed in duplicate or triplicate.

Figure S2. Purification, cryo-EM data imaging and processing of GLP-1R:G_s complexes. *Related to Figures 2 and 3*. **Top,** GLP-1 bound complex; **Middle**, PF 06882961 bound complex; **Bottom,** OWL-833 bound complex. Within each panel: Top left, size exclusion chromatography profile and Coomassie gel of the purified complex. Top middle, 3-D histogram representation of the Euler angle distribution of all the particles used in the reconstruction overlaid on the density map drawn on the same coordinate axis. Top right; exemplar micrograph and 2D class averages of cryo-EM projections of the complex. Bottom left, Gold standard Fourier shell correlation (FSC) curves for the final consensus maps and map validation from half maps, showing the overall nominal resolution. Bottom middle-right, Local resolution-filtered EM maps (consensus and receptor/ECD focused refinements) displaying local resolution (Å) coloured from highest resolution (dark blue) to lowest resolution (red).

Figure S3. Atomic models of the ligands, receptors and $G\alpha_s$ α5 helix in the cryo-EM map. *Related to Figures 2, 3, 6 & S7*. EM density map and the model are shown for GLP-1, PF 06882961, OWL-833 and all seven TM helices, and ECLs of the GLP-1R when bound to each agonist. The α5 helix of the $G\alpha_S$ Ras-like domain is also shown for each complex. For GLP-1R, the consensus map was used, with the exception of those labelled * where the ECD refined map is shown. For PF 06882961- and OWL-833 receptor and ligand density was from the receptor-focused refined maps. For the α5 helix, all density shown is from the consensus cryo-EM maps for the respective complex. ECL3 for OWL-833 was poorly resolved and was not modelled.

Figure S4. Ligand interactions with the GLP-1R. *Related to Figure 3.* **A,** Overlay of 5VAI with the 2.1 Å GLP-1 bound GLP-1R structure reveals differences within the extracellular region between the two structures. These reveal differences in modelled interactions between GLP-1 and residues within TM1, ECL2/TM5 and TM6/ECL3/TM7. **B,** Top, interactions between the N-terminal portion of GLP-1 (residues 7-17) and the GLP-1R TM bundle as determined by Ligplot+. Middle; Atomic models of the binding sites of the PF-06882961-, GLP-1- and OWL-833- bound GLP-1Rs and their density within the cryo-EM maps. Bottom, interactions between PF 06882961 (left) and OWL-833 (right) with the GLP-1R as determined by Ligplot+. In the Ligplot+ figures, hydrogen bonds are shown as green dotted lines, whereas red dotted lines are hydrophobic contacts. Blue spheres indicate waters that directly interact with ligands.

Figure S5. Ligand mediated cAMP accumulation in ChoFlpIn cells stably expressing WT or mutant hGLP-1Rs. *Related to Figures 3, 4 and 6.* Concentration response curves for alanine mutants of the GLP-1R were assessed for GLP-1, PF 06882961 and OWL-833. Residues that either interacted with PF 06882961, OWL-833 or both agonists were selected to assess their importance in ligand-mediated receptor activity. A select set of residues that interact with peptide in the GLP-1 bound structure, but with water in the cryo-EM structures of the GLP-1R bound to PF 06882961 and OWL-833 (right) were also assessed. All data are the means + S.E.M of at least four independent experiments performed in duplicate.

Figure S6. The GLP-1R binding pocket shape, volume and properties differ in the presence of different agonists. *Related to Figures 4, 5 and Video S1.* **A,** Slice through of the upper portion of TM bundles bound to different agonists, coloured by hydrophobicity (top) and electrostatic potential (bottom). **B,** Overlay of OWL-833-bound structure with 6ORV (TT-OAD2 bound GLP-1R structure) revealed significant overlap in the ligand binding poses and commonalities in the conformation of TM6 and 7. **C,** Overlay of GLP-1-bound (orange), ExP5 bound (6B3J – yellow), OWL-833-bound (pale blue) and TT-OAD2 bound (6ORV – cornflower blue) GLP-1R structures shows differences in the TM6-ECL3-TM7 conformation.

Figure S7. The GLP-1R:G_s complexes bound by different agonists share common interactions with G_s, yet differences in the mobility of the $G\alpha_s$ AHD. *Related to Figures 4 and 5 and Videos S3 and S4.* **Top,** superimposition of the GLP-1-bound (orange), PF 06882961-bound (pale green) and OWL-833-bound (pale blue) GLP-1R:G_s complexes reveal identical backbone conformations within the intracellular portion of the TM bundle, the G protein and the G protein: receptor interface. Rotamer positions of side chains in the lower portion of the receptor bundle were also conserved in the three structures (not shown). **Middle**; Interactions formed between the GLP-1R (orange) and the G protein (α - gold (right), β-cyan (left)) in the GLP-1 bound GLP-1R structure. Identical interactions were observed in the other two structures, including water (red spheres) mediated interactions. Middle panel shows a cut through of the model with the cryo-EM density showing the G protein:receptor interface. **Bottom,** 3D classification using a mask of the $G\alpha_s$, including AHD, revealed multiple conformations of this domain relative to the Ras domain. 3 common classes were observed in all three GLP-1R complexes (purple – "open/up", yellow – "mid" and coral – "closed/down", however, the % of particles in each class differed depending on the bound ligand; these are shown above the 3D classes. The other two classes differed between complexes and had less well-defined AHDs. The total number of particles used for the 3D classification were 615K, 732K, 933K for GLP-1, PF 06882961 and OWL-833, respectively. While not the most populated, the down conformation (coral) was the only class of sufficient resolution to enable modelling of the AHD and this is shown in panel A.

Video S1. GLP-1, PF 06882961 and OWL-833 stabilise distinct binding pocket volumes within the GLP-1R. *Related to Figures 3-5 and S6.* Slice through the centre of the GLP-1R bundles bound by different agonists, with a 360° y axis rotation around the centre of each receptor bundle. This highlights distinctions in the volume and shapes of GLP-1R TM domain (TMD) binding cavities of GLP-1, PF 06882961 and OWL-833.

Video S2. Morphs between the inactive and distinct agonist-bound GLP-1R conformations. *Related to Figure 5.* Morphs between the inactive GLP-1R (6LN2) and agonist-bound conformations (GLP-1, PF 06882961, OWL-833 and TT-OAD2 (6ORV).

Video S3. 3D Variability analysis of GLP-1 and non-peptidic agonist bound GLP-1R:G_s complexes. *Related to Figure 2 and 7.* CryoSPARC variability analysis performed on the GLP-

1R:G_s complexes in the presence of different bound agonists. Transition 1: Principal component 1; Transition 2: Principal component 2; Transition 3; Principal component 3; Transition 4: Static backbone models built into the cryo-EM maps from frame 000 and frame 019 from Principal component 1 of the GLP-1-bound GLP-1R analysis revealed 7.1 - 7.3 Å differences between the maps (when measured from the Cα of $D215^{ECL1}$ and $T51^{ECD}$), highlighting the coordinated movements within ECL1 and the ECD. These were associated with a 4.5 Å movement within the C-terminus of GLP-1 (measured from the Cα of $K34^{GLP\text{-}1}$).

Video S4. 3D Variability analysis reveals differences in the GLP-1 ECD and G_s AHD dynamics in the presence of different agonists. *Related to Figures 4, 7 and S7.* Transition 1 shows the cryoSPARC 3D variability analysis performed on each complex. This shows substantial mobility in the G_s AHD when the GLP-1R is bound by GLP-1, PF 06882961 and OWL-833, but less mobility in the TT-OAD2 bound complex. In contrast, while the GLP-1R ECD is relatively stable in the PF 06882961, OWL-833 and to a lesser extent GLP-1 bound complexes, this domain is extremely mobile when bound by TT-OAD2. Transition 2 shows morphs between the three common conformations of the G_s AHD location for the GLP-1, PF 06882961 and OWL-833 bound GLP-1R:G_s complexes determined from 3D classification using a mask of $G\alpha_s$, including the AHD.

Figure S1

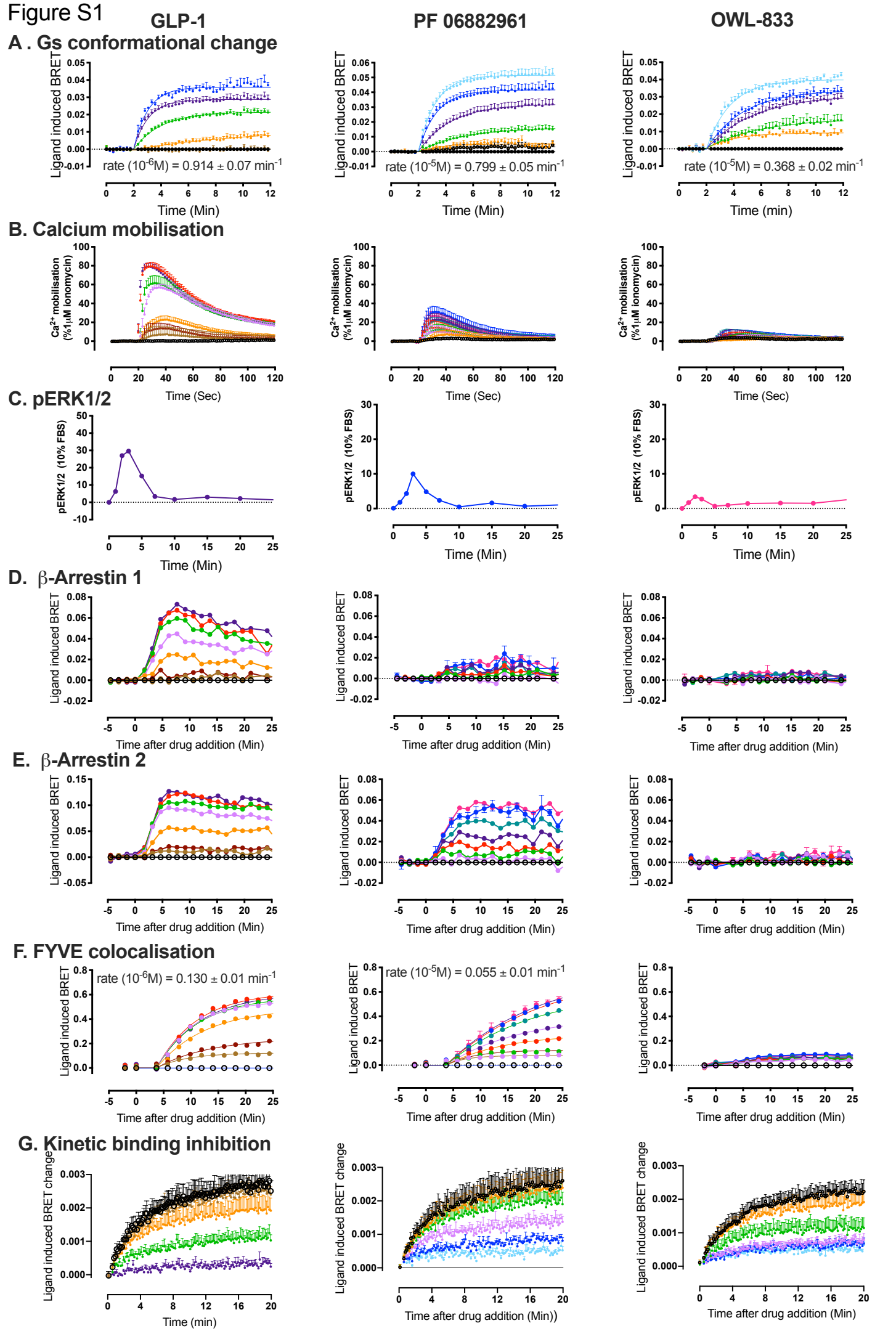
GLP-1
PF 06882961
OWL-833
A . Gs conformational change
Ligand induced BRET
rate (10^{-6}M) = 0.914 ± 0.07 min^{-1}
rate (10^{-5}M) = 0.799 ± 0.05 min^{-1}
rate (10^{-5}M) = 0.368 ± 0.02 min^{-1}
Time (Min)
Time (min)
B. Calcium mobilisation
Ca2+ mobilisation (%1μM ionomycin)
Time (Sec)
C. pERK1/2
pERK1/2 (10% FBS)
Time (Min)
D. β-Arrestin 1
Ligand induced BRET
Time after drug addition (Min)
E. β-Arrestin 2
Ligand induced BRET
Time after drug addition (Min)
F. FYVE colocalisation
rate (10^{-6}M) = 0.130 ± 0.01 min^{-1}
rate (10^{-5}M) = 0.055 ± 0.01 min^{-1}
Ligand induced BRET
Time after drug addition (Min)
G. Kinetic binding inhibition
Ligand induced BRET change
Time (min)
Time after drug addition (Min))
Time after drug addition (Min)
Ligand Concentrations: 1nM 3nM. 10nM. 30nM. 100nM. 300nM. 1μM. 3μM. 10μM. 30μM. 100μM

Figure S2

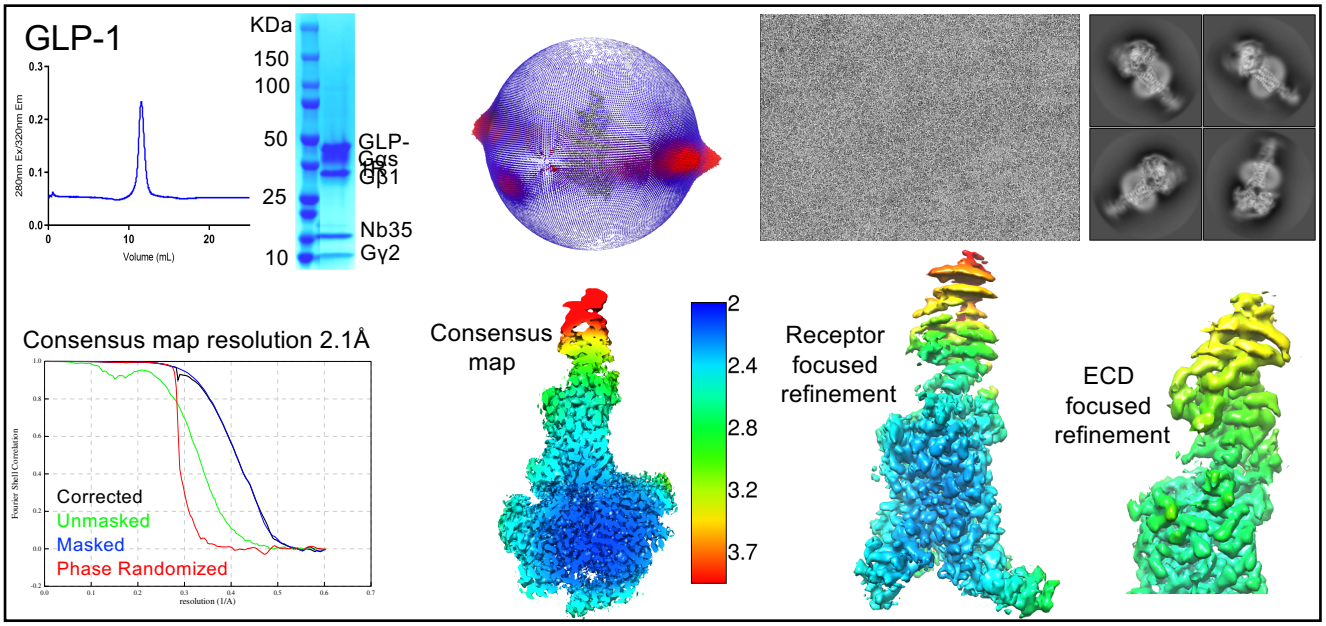
GLP-1
280nm Ex/320nm Em
Volume (mL)
KDa
150
100
50
25
10
GLP-
Gαs
Gβ1
Nb35
Gγ2
Consensus map resolution 2.1Å
Fourier Shell Correlation
Corrected
Unmasked
Masked
Phase Randomized
resolution (1/Å)
Consensus map
2
2.4
2.8
3.2
3.7
Receptor focused refinement
ECD focused refinement

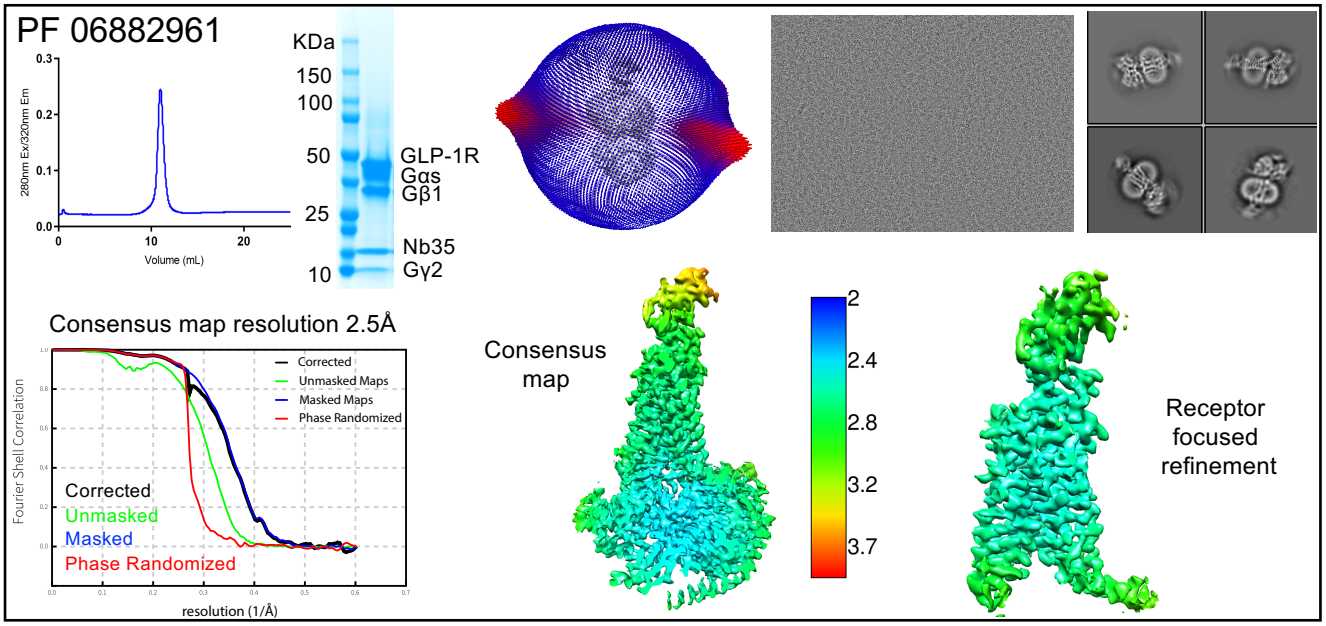
PF 06882961
280nm Ex/320nm Em
Volume (mL)
KDa
150
100
50
25
10
GLP-1R
Gαs
Gβ1
Nb35
Gγ2
Consensus map resolution 2.5Å
Fourier Shell Correlation
Corrected
Unmasked Maps
Masked Maps
Phase Randomized
Corrected
Unmasked
Masked
Phase Randomized
resolution (1/Å)
Consensus map
2
2.4
2.8
3.2
3.7
Receptor focused refinement

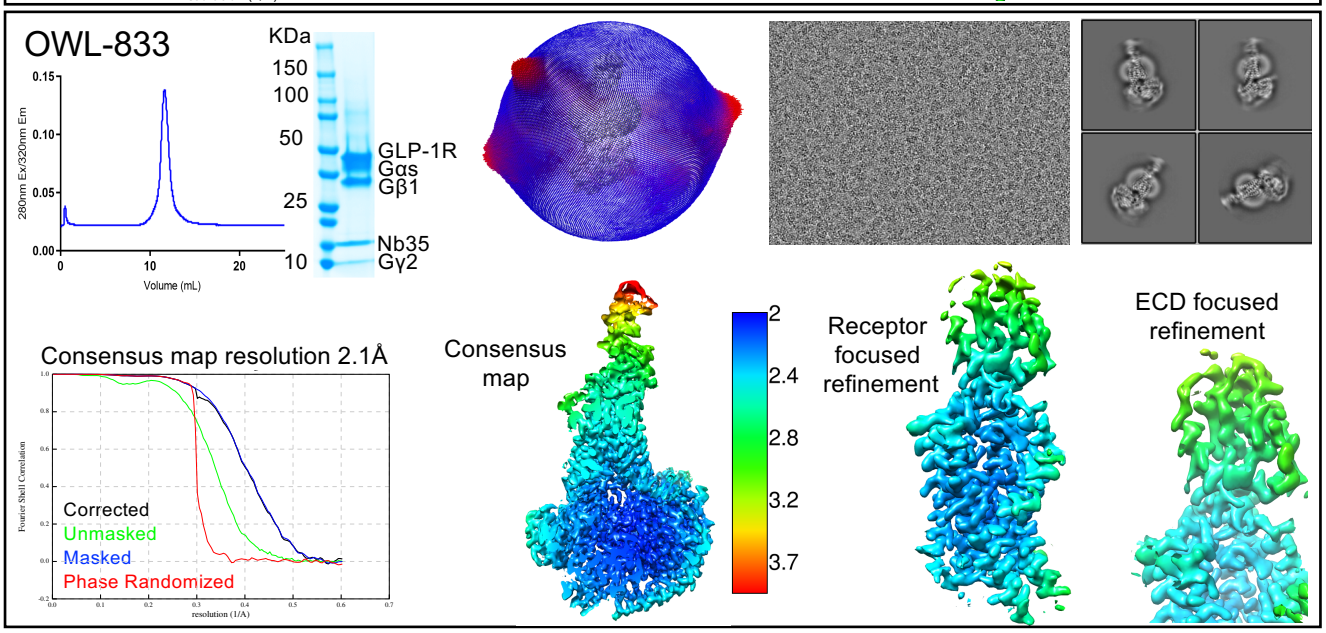
OWL-833
280nm Ex/320nm Em
Volume (mL)
KDa
150
100
50
25
10
GLP-1R
Gαs
Gβ1
Nb35
Gγ2
Consensus map resolution 2.1Å
Fourier Shell Correlation
Corrected
Unmasked
Masked
Phase Randomized
resolution (1/Å)
Consensus map
2
2.4
2.8
3.2
3.7
Receptor focused refinement
ECD focused refinement

Figure S3

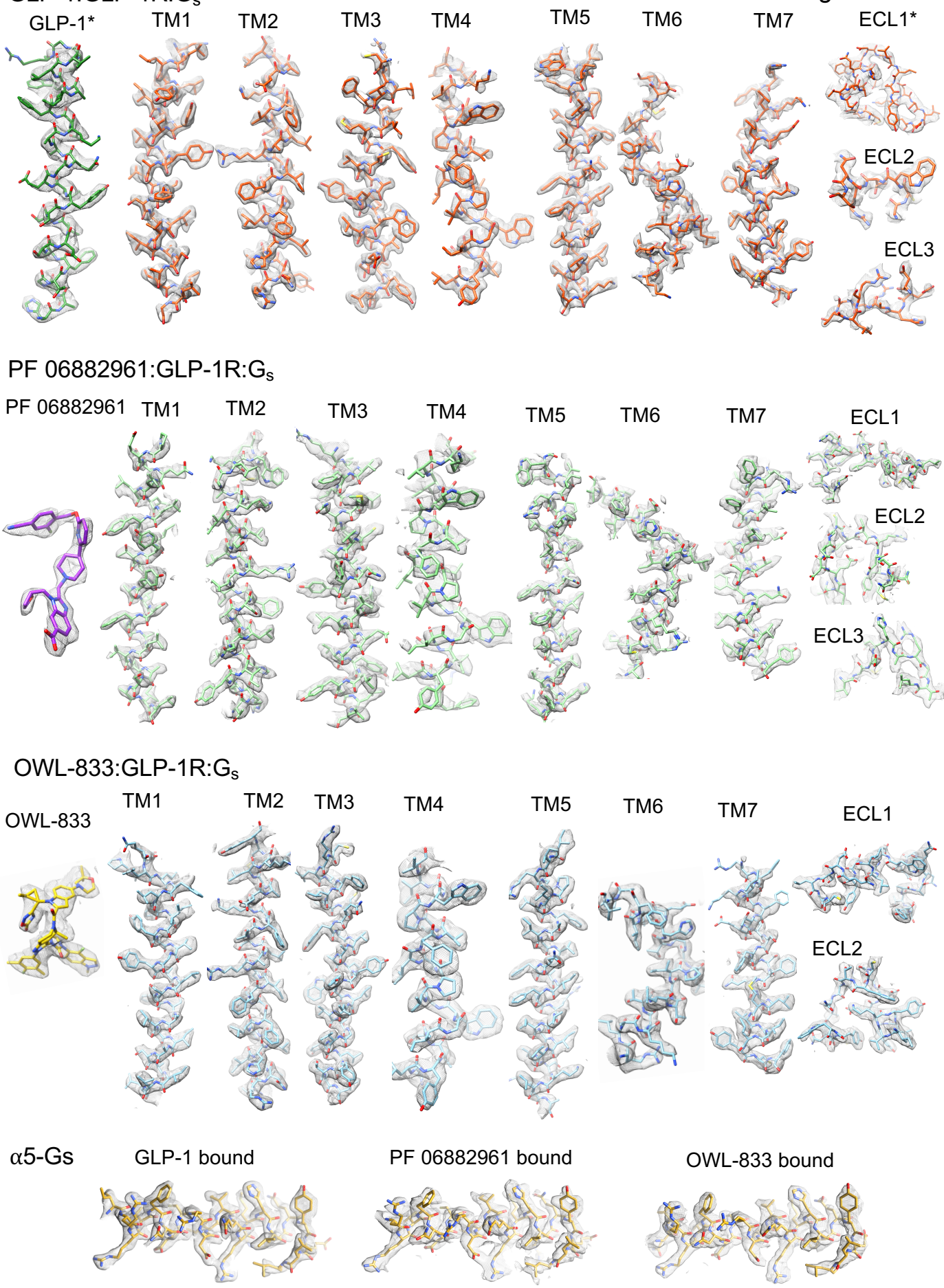
GLP-1:GLP-1R:Gs
GLP-1*
TM1
TM2
TM3
TM4
TM5
TM6
TM7
ECL1*
ECL2
ECL3
PF 06882961:GLP-1R:Gs
PF 06882961
TM1
TM2
TM3
TM4
TM5
TM6
TM7
ECL1
ECL2
ECL3
OWL-833:GLP-1R:Gs
OWL-833
TM1
TM2
TM3
TM4
TM5
TM6
TM7
ECL1
ECL2
α5-Gs
GLP-1 bound
PF 06882961 bound
OWL-833 bound

Figure S4

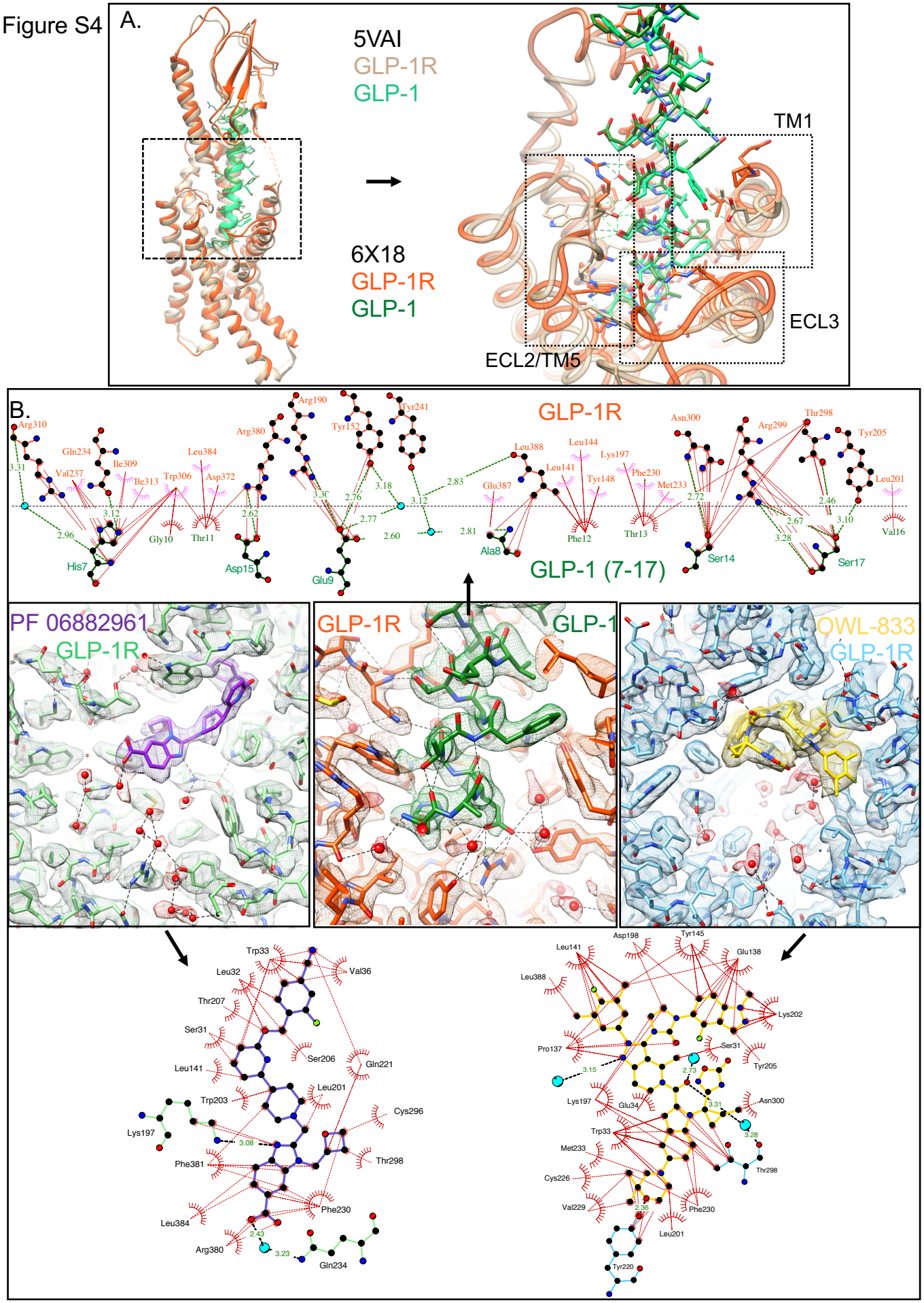
A.
5VAI
GLP-1R
GLP-1
6X18
GLP-1R
GLP-1
TM1
ECL3
ECL2/TM5
B.
GLP-1R
GLP-1 (7-17)
Arg310
Gln234
Val237
Ile309
Ile313
Trp306
Leu384
Asp372
Arg380
Arg190
Tyr152
Tyr241
His7
Gly10
Thr11
Asp15
Glu9
Leu388
Leu144
Leu141
Lys197
Tyr148
Glu387
Phe230
Met233
Thr13
Ala8
Phe12
Asn300
Arg299
Thr298
Tyr205
Leu201
Ser14
Ser17
Val16
PF 06882961
GLP-1R
GLP-1R
GLP-1
OWL-833
GLP-1R
Trp33
Leu32
Val36
Thr207
Ser31
Ser206
Gln221
Leu141
Leu201
Trp203
Cys296
Lys197
Phe381
Thr298
Phe230
Leu384
Arg380
Gln234
Asp198
Tyr145
Leu141
Glu138
Leu388
Lys202
Pro137
Ser31
Tyr205
Lys197
Glu34
Asn300
Trp33
Met233
Thr298
Cys226
Val229
Phe230
Leu201
Tyr220

Figure S5

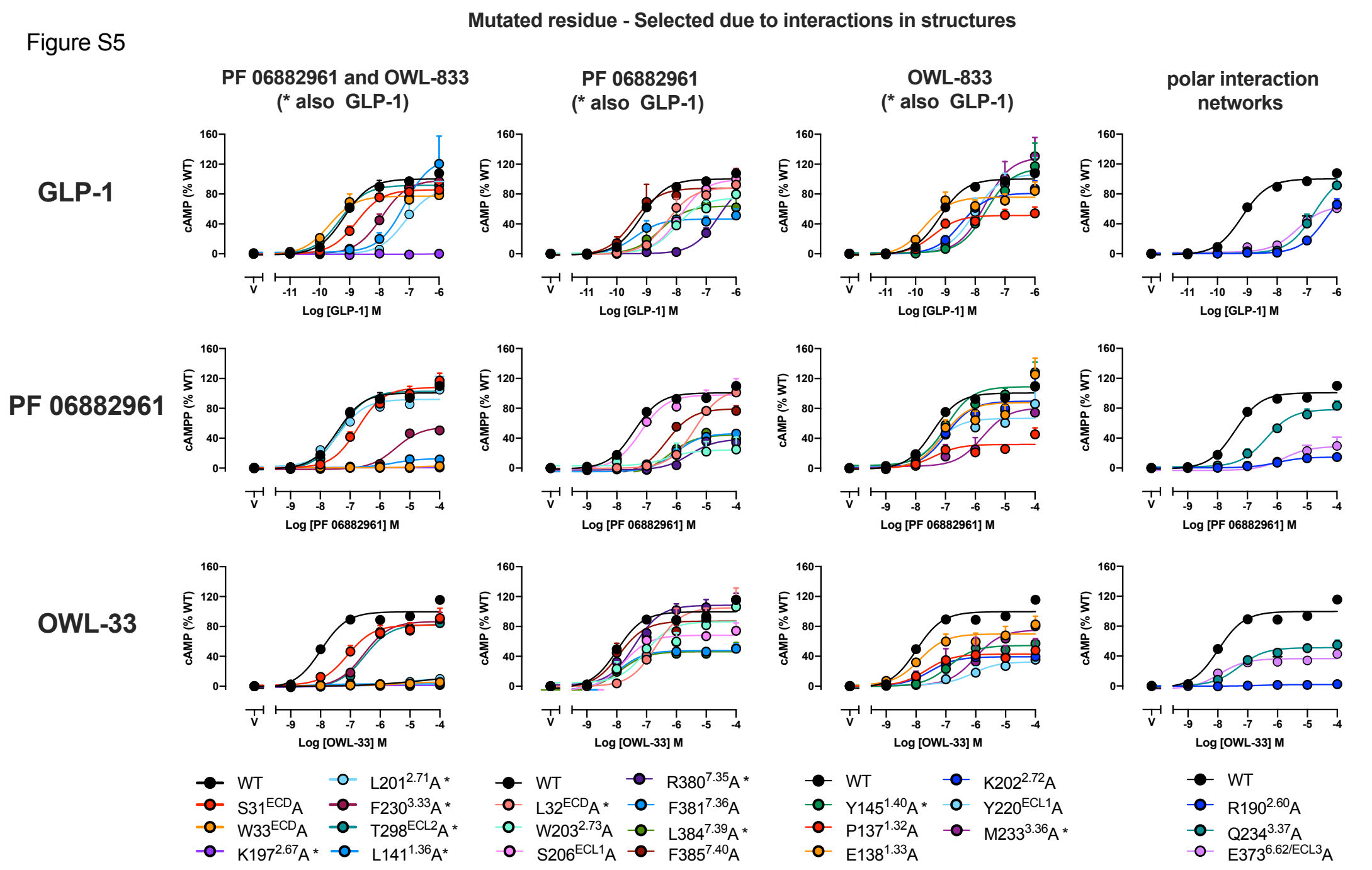
Mutated residue - Selected due to interactions in structures
PF 06882961 and OWL-833
(* also GLP-1)
PF 06882961
(* also GLP-1)
OWL-833
(* also GLP-1)
polar interaction networks
GLP-1
PF 06882961
OWL-33
cAMP (% WT)
cAMPP (% WT)
Log [GLP-1] M
Log [PF 06882961] M
Log [OWL-33] M
WT
S31ECDA
W33ECDA
K1972.67A *
L2012.71A *
F2303.33A *
T298ECL2A *
L1411.36A*
WT
L32ECDA *
W2032.73A
S206ECL1A
R3807.35A *
F3817.36A
L3847.39A *
F3857.40A
WT
Y1451.40A *
P1371.32A
E1381.33A
K2022.72A
Y220ECL1A
M2333.36A *
WT
R1902.60A
Q2343.37A
E373 6.62/ECL3A

Figure S6

A.

Hydrophobicity min – blue none – white max - orange

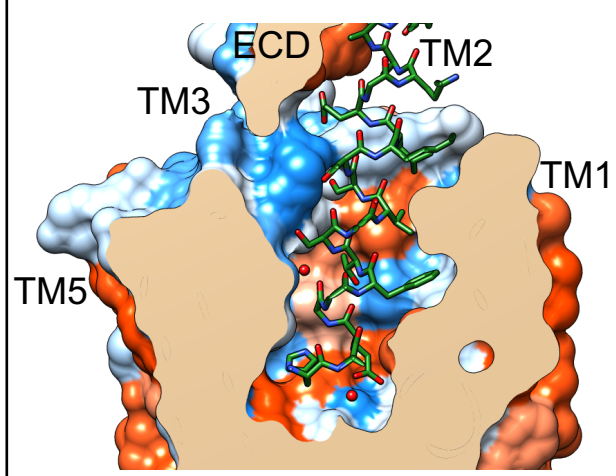

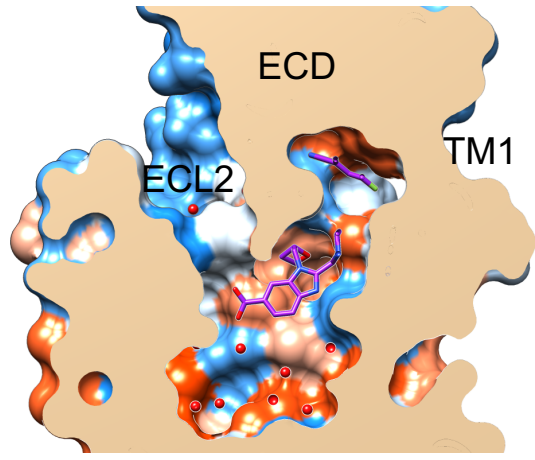

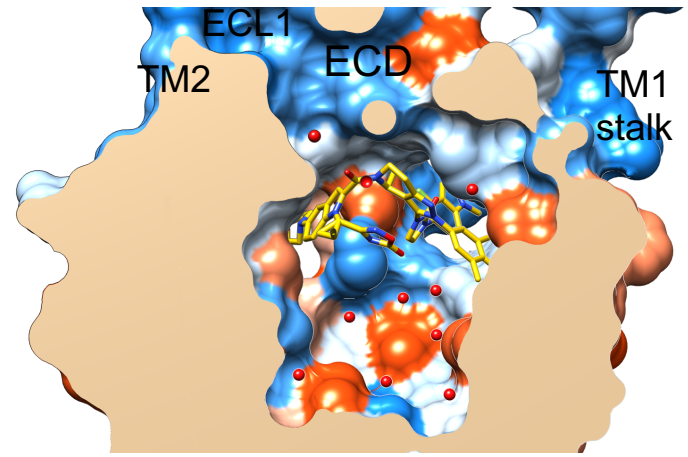

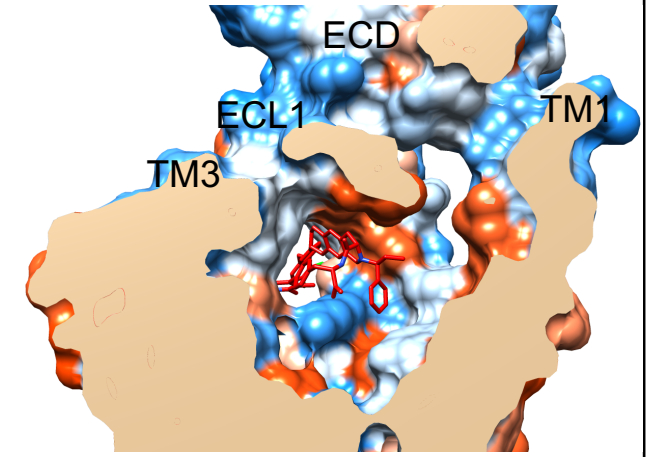

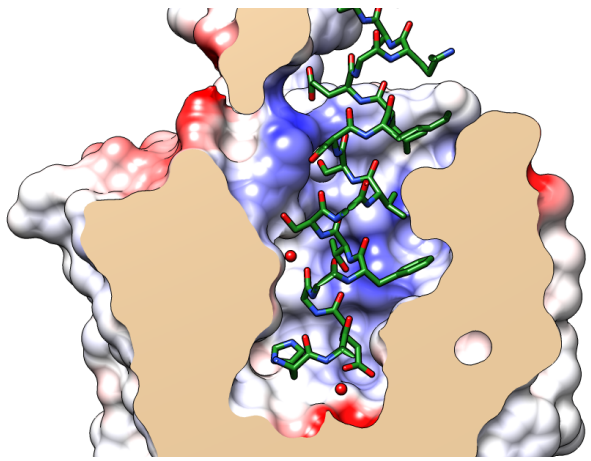

GLP-1

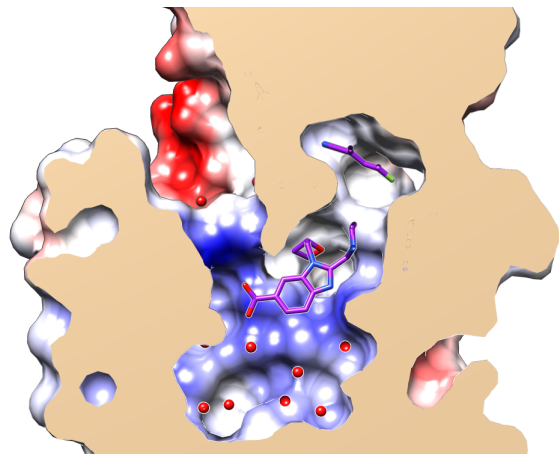

PF 06882961

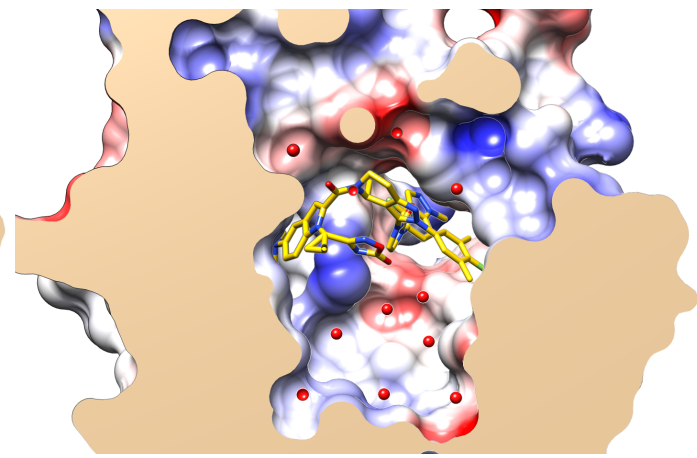

OWL-833

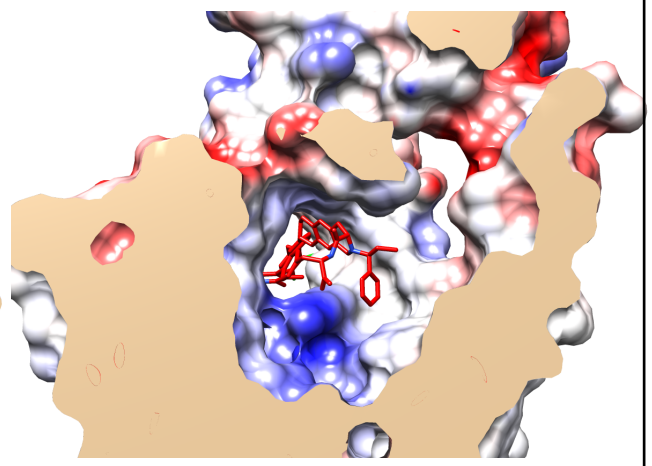

TT-OAD2

Electrostatic Potential +ve-blue neutral-white -ve- red

B.

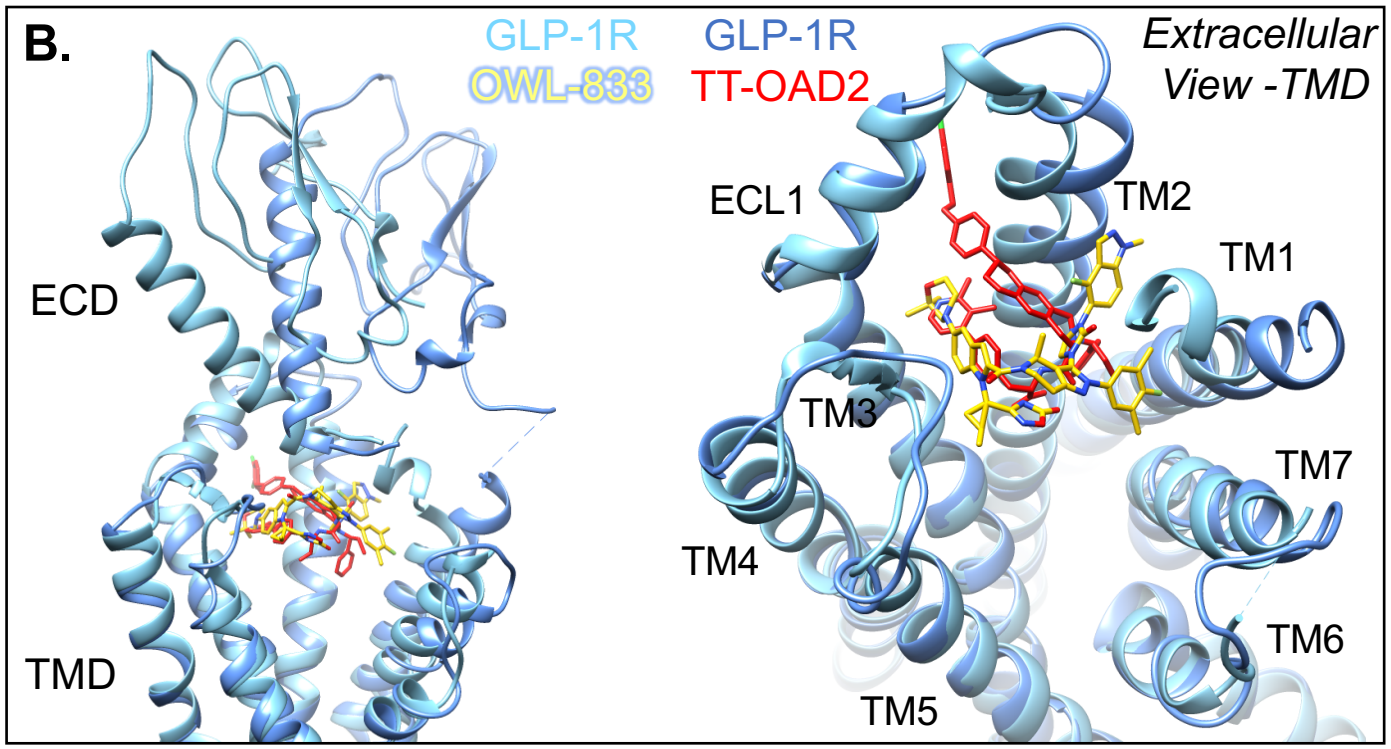

C.

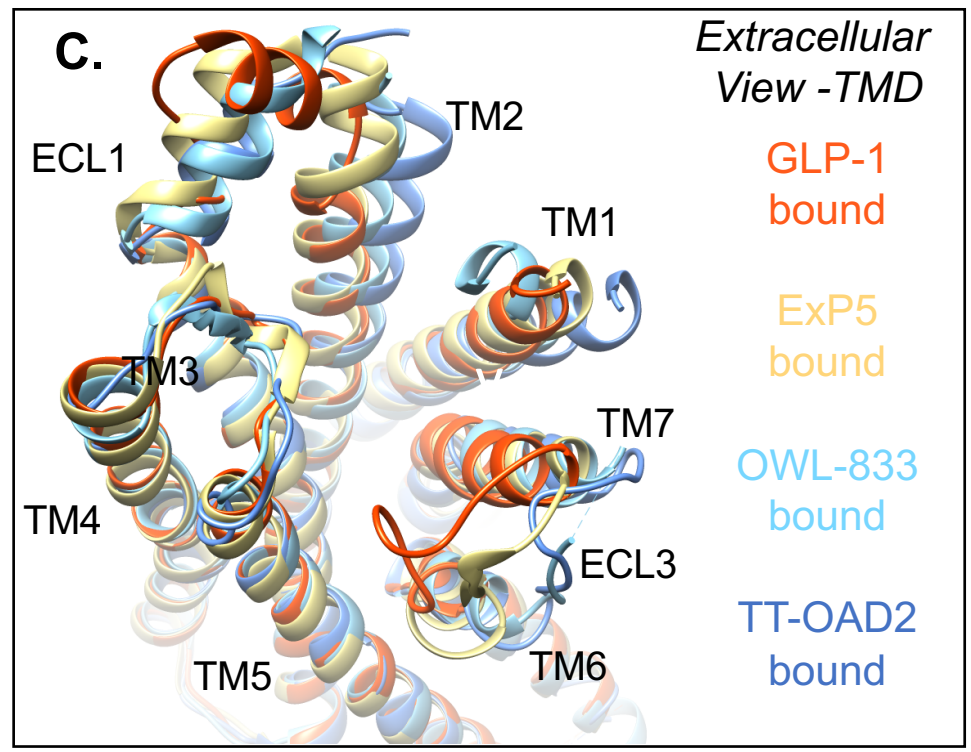

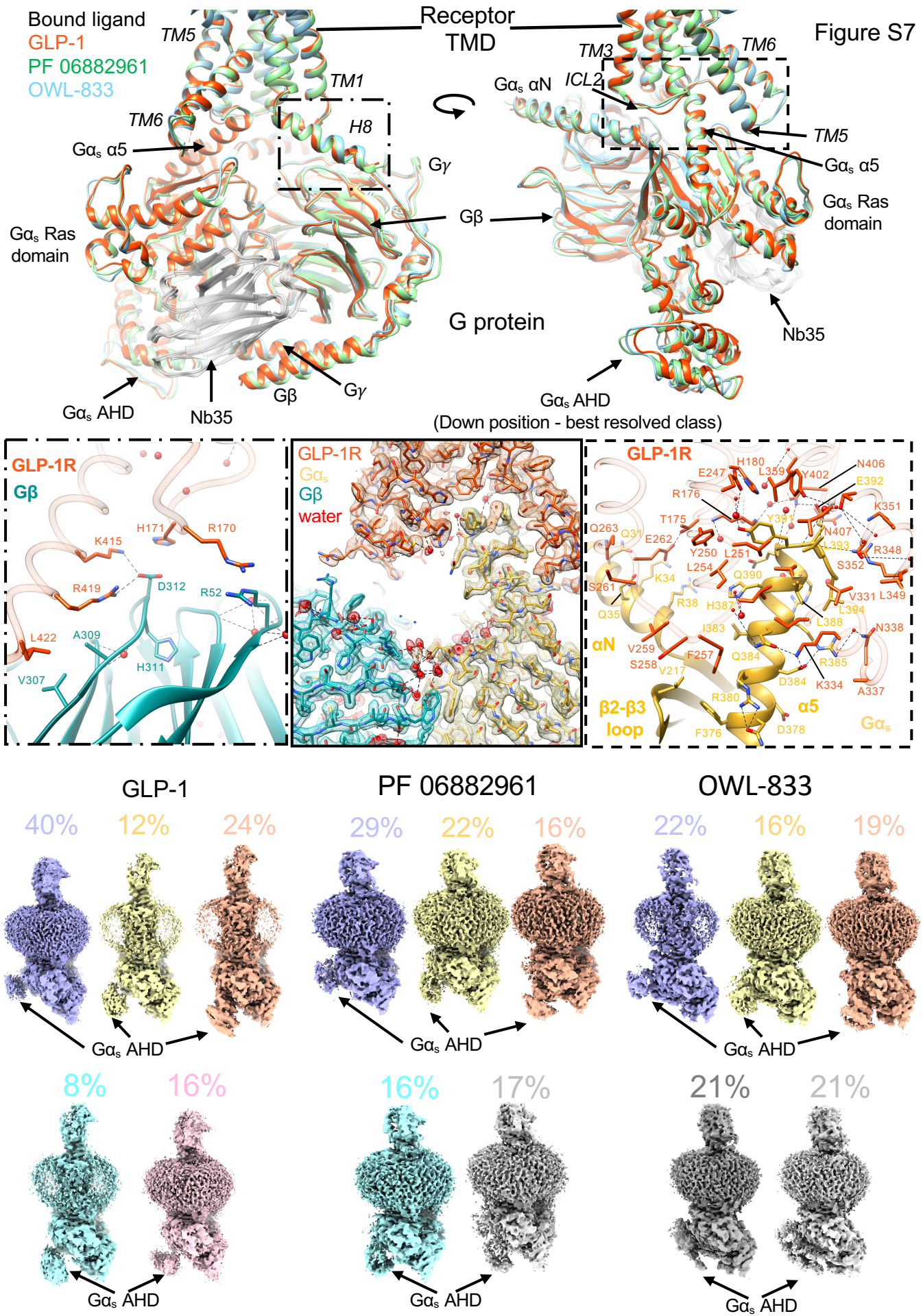
Figure S7
Bound ligand
GLP-1
PF 06882961
OWL-833
Receptor TMD
TM5
TM1
TM6
H8
Gαs α5
Gγ
Gβ
Gαs Ras domain
Gαs AHD
Nb35
TM3
TM6
Gαs αN
ICL2
TM5
Gαs α5
Gαs Ras domain
Nb35
G protein
(Down position - best resolved class)
GLP-1R
Gβ
H171
R170
K415
R419
D312
R52
L422
A309
H311
V307
GLP-1R
Gαs
Gβ
water
GLP-1R
H180
E247
L359
Y402
N406
E392
R176
K351
T175
Y391
Q263
Q31
E262
N407
L393
R348
Y250
L251
S352
L254
Q390
S261
K34
V331
L349
R38
H387
L394
Q35
L388
I383
N338
αN
V259
F257
Q384
R385
S258
V217
D384
K334
A337
R380
β2-β3 loop
α5
Gαs
F376
D378
GLP-1
PF 06882961
OWL-833
40%
12%
24%
29%
22%
16%
22%
16%
19%
Gαs AHD
Gαs AHD
Gαs AHD
8%
16%
16%
17%
21%
21%
Gαs AHD
Gαs AHD
Gαs AHD